RESEARCH ARTICLE SUMMARY

PLASMA ASTROPHYSICS

Electron-scale measurements of magnetic reconnection in space

J. L. Burch,* R. B. Torbert, T. D. Phan, L.-J. Chen, T. E. Moore, R. E. Ergun, J. P. Eastwood, D. J. Gershman, P. A. Cassak, M. R. Argall, S. Wang, M. Hesse, C. J. Pollock, B. L. Giles, R. Nakamura, B. H. Mauk, S. A. Fuselier, C. T. Russell, R. J. Strangeway, J. F. Drake, M. A. Shay, Yu. V. Khotyaintsev, P.-A. Lindqvist, G. Marklund, F. D. Wilder, D. T. Young, K. Torkar, J. Goldstein, J. C. Dorelli, L. A. Avanov, M. Oka, D. N. Baker, A. N. Jaynes, K. A. Goodrich, I. J. Cohen, D. L. Turner, J. F. Fennell, J. B. Blake, J. Clemmons, M. Goldman, D. Newman, S. M. Petrinec, K. J. Trattner, B. Lavraud, P. H. Reiff, W. Baumjohann, W. Magnes, M. Steller, W. Lewis, Y. Saito, V. Coffey, M. Chandler

INTRODUCTION: Magnetic reconnection is a physical process occurring in plasmas in which magnetic energy is explosively converted into heat and kinetic energy. The effects of reconnection—such as solar flares, coronal mass ejections, magnetospheric substorms and auroras, and astrophysical plasma jets—have been studied theoretically, modeled with computer simulations, and observed in space. However, the electron-scale kinetic physics, which controls how magnetic field lines break and reconnect, has up to now eluded observation.

RATIONALE: To advance understanding of magnetic reconnection with a definitive experiment in space, NASA developed and launched the Magnetospheric Multiscale (MMS) mission in March 2015. Flying in a tightly controlled tetrahedral formation, the MMS spacecraft can sample the magnetopause, where the interplanetary and geomagnetic fields reconnect, and make detailed measurements of the plasma environment and the electric and magnetic fields in the reconnection region. Because the reconnection dissipation region at the magnetopause is thin (a few kilometers) and moves rapidly back and forth across the spacecraft (10 to 100 km/s), high-resolution measurements are needed to capture the microphysics of reconnection. The most critical measurements are of the three-dimensional electron distributions, which must be made every 30 ms, or 100 times the fastest rate previously available.

RESULTS: On 16 October 2015, the MMS tetrahedron encountered a reconnection site on the dayside magnetopause and observed (i) the conversion of magnetic energy to particle kinetic energy; (ii) the intense current and electric field that causes the dissipation of magnetic energy; (iii) crescent-shaped electron velocity distributions that carry the current; and (iv) changes in magnetic topology. The crescent-shaped features in the velocity distributions (left side of the figure) are the result of demagnetization of solar wind electrons as they flow into the reconnection site, and their acceleration and deflection by an outward-pointing electric field that is set up at the magnetopause boundary by plasma density gradients. As they are deflected in these fields, the solar wind electrons mix in with magnetospheric electrons and are accelerated along a meandering path that straddles the boundary, picking up the energy released in annihilating the magnetic field. As evidence of the predicted interconnection of terrestrial and solar wind magnetic fields, the crescent-shaped velocity distributions are diverted along the newly connected magnetic field lines in a narrow layer just at the boundary. This diversion along the field is shown in the right side of the figure.

ON OUR WEBSITE

Read the full article at http://dx.doi.org/10.1126/science.aaf2939

CONCLUSION: MMS has yielded insights into the microphysics underlying the reconnection between interplanetary and terrestrial magnetic fields. The persistence of the characteristic crescent shape in the electron distributions suggests that the kinetic processes causing magnetic field line reconnection are dominated by electron dynamics, which produces the electric fields and currents that dissipate magnetic energy. The primary evidence for this magnetic dissipation is the appearance of an electric field and a current that are parallel to one another and out of the plane of the figure. MMS has measured this electric field and current, and has identified the important role of electron dynamics in triggering magnetic reconnection. ■

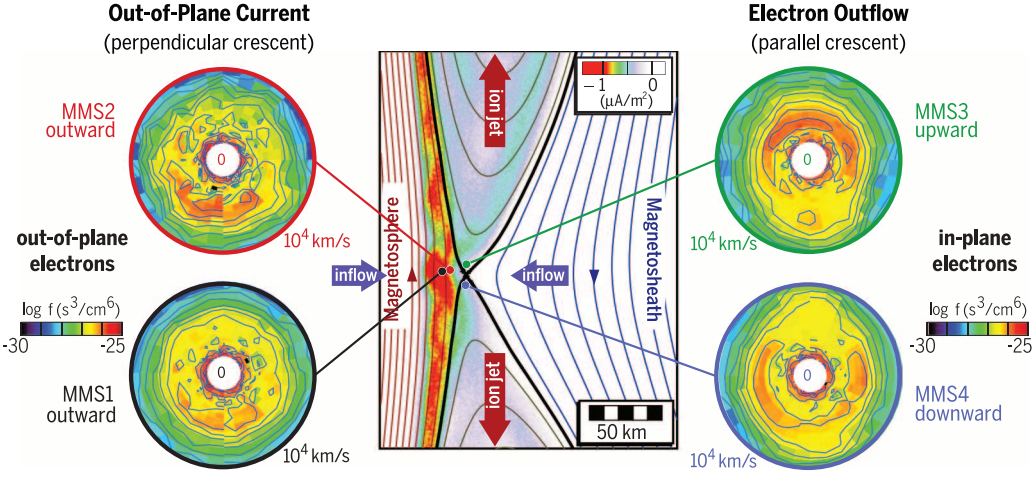

Electron dynamics controls the reconnection between the terrestrial and solar magnetic fields. The process of magnetic reconnection has been a long-standing mystery. With fast particle measurements, NASA's Magnetospheric Multiscale (MMS) mission has measured how electron dynamics controls magnetic reconnection. The data in the circles show electrons with velocities from 0 to 10^4 km/s carrying current out of the page on the left side of the X-line and then flowing upward and downward along the reconnected magnetic field on the right side. The most intense fluxes are red and the least intense are blue. The plot in the center shows magnetic field lines and out-of-plane currents derived from a numerical plasma simulation using the parameters observed by MMS.

The list of author affiliations is available in the full article online.
*Corresponding author. Email: jburch@swri.edu
Cite this article as J. L. Burch *et al.*, *Science* 352, aaf2939 (2016). DOI: 10.1126/science.aaf2939

RESEARCH ARTICLE

PLASMA ASTROPHYSICS

Electron-scale measurements of magnetic reconnection in space

J. L. Burch,[1]* R. B. Torbert,[1,2] T. D. Phan,[3] L.-J. Chen,[4] T. E. Moore,[5] R. E. Ergun,[6] J. P. Eastwood,[7] D. J. Gershman,[5] P. A. Cassak,[8] M. R. Argall,[2] S. Wang,[4] M. Hesse,[5] C. J. Pollock,[5] B. L. Giles,[5] R. Nakamura,[9] B. H. Mauk,[10] S. A. Fuselier,[1] C. T. Russell,[11] R. J. Strangeway,[11] J. F. Drake,[4] M. A. Shay,[12] Yu. V. Khotyaintsev,[13] P.-A. Lindqvist,[14] G. Marklund,[14] F. D. Wilder,[6] D. T. Young,[1] K. Torkar,[9] J. Goldstein,[1] J. C. Dorelli,[5] L. A. Avanov,[5] M. Oka,[3] D. N. Baker,[6] A. N. Jaynes,[6] K. A. Goodrich,[6] I. J. Cohen,[10] D. L. Turner,[15] J. F. Fennell,[15] J. B. Blake,[15] J. Clemmons,[15] M. Goldman,[16] D. Newman,[16] S. M. Petrinec,[17] K. J. Trattner,[6] B. Lavraud,[18] P. H. Reiff,[19] W. Baumjohann,[9] W. Magnes,[9] M. Steller,[9] W. Lewis,[1] Y. Saito,[20] V. Coffey,[21] M. Chandler[21]

Magnetic reconnection is a fundamental physical process in plasmas whereby stored magnetic energy is converted into heat and kinetic energy of charged particles. Reconnection occurs in many astrophysical plasma environments and in laboratory plasmas. Using measurements with very high time resolution, NASA's Magnetospheric Multiscale (MMS) mission has found direct evidence for electron demagnetization and acceleration at sites along the sunward boundary of Earth's magnetosphere where the interplanetary magnetic field reconnects with the terrestrial magnetic field. We have (i) observed the conversion of magnetic energy to particle energy; (ii) measured the electric field and current, which together cause the dissipation of magnetic energy; and (iii) identified the electron population that carries the current as a result of demagnetization and acceleration within the reconnection diffusion/dissipation region.

Magnetic reconnection is an energy conversion process that operates in many astrophysical environments, producing energetic phenomena such as geomagnetic storms and aurora, solar flares and coronal mass ejections, x-ray flares in magnetars, and magnetic interactions between neutron stars and their accretion disks. Reconnection is also crucially important in laboratory plasma physics, where it has proved to be an impediment to the achievement of magnetic-confinement fusion through the sawtooth crashes that it triggers. A better understanding of reconnection is an important goal for plasma physics on Earth and in space, but a complete experiment is impossible to conduct in most environments, which are too distant, too hot, or too small for comprehensive in situ measurements (*1*).

Earth's magnetosphere has been explored by many spacecraft missions, some of which have made multipoint measurements in and around regions containing collisionless magnetic reconnection (*2*–*7*). Results from these missions have verified many of the predictions about magnetic reconnection phenomena on the magnetohydrodynamic (MHD) and ion scales. However, to make major progress in the study of collisionless reconnection in space, it is necessary to extend the measurements to the electron scale and make accurate three-dimensional measurements of electric and magnetic fields. Also required are accurate ion composition measurements, which can help to determine the role of ionospheric particles in reconnection, as well as energetic particle measurements, which can help to determine where magnetic fields interconnect and how particles are accelerated to high energies.

NASA's Magnetospheric Multiscale (MMS) mission (*8*) was designed to perform a definitive experiment in space on magnetic reconnection at the electron scale, at which dissipation of magnetic energy and the resulting interconnection of magnetic fields occur. Electron-scale kinetic physics in the region around the reconnection site (or the X-line) where field line breaking and reconnection occur has not previously been investigated experimentally in space, owing to insufficiently detailed measurements. Our knowledge of this region at the electron scale has come mainly from computer simulations (*9*–*13*) and laboratory experiments (*14*, *15*). The higher resolution of MMS measurements in both time and space relative to previous missions offers an opportunity to investigate the cause of reconnection by resolving the structures and dynamics within the X-line region.

The data set obtained by MMS incorporates the following advances: (i) four spacecraft in a closely controlled tetrahedron formation with adjustable separations down to 10 km; (ii) three-axis electric and magnetic field measurements with accurate cross-calibrations allowing for the measurement of spatial gradients and time variations; and (iii) all-sky plasma electron and ion velocity-space distributions with time resolution of 30 ms for electrons and 150 ms for ions.

The four MMS spacecraft were launched together on 13 March 2015 (UT) into a highly elliptical (inclination 28°) orbit with perigee at 1.2 Earth radii (R_E) and apogee at 12 R_E (both geocentric). The mission is being conducted in two phases, the first phase targeting the dayside outer boundary of Earth's magnetosphere (the magnetopause) and the second phase targeting the geomagnetic tail, for which the apogee is raised to 25 R_E. This article focuses on magnetopause measurements during the first science phase of the mission, which began on 1 September 2015. For this phase, a region of interest was identified as geocentric radial distances of 9 to 12 R_E, during which all instruments are operated at their fastest cadence, producing burst-mode data. Within the region of interest, the four spacecraft are maintained in a tetrahedral formation with separations variable between 160 and 10 km. A quality factor for the tetrahedra, defined by the ratio of their surface area to their volume, is maintained to within 80% of the ratio for a regular tetrahedron.

By 14 December 2015, the spacecraft had crossed the magnetopause more than 2000 times. On the basis of detection of plasma jetting and heating within the magnetopause current sheets, we infer that at least 50% of the crossings encountered magnetic reconnection. Most crossings occurred in the reconnection exhaust downstream of the X-line, but a few of them passed very close to the X-line. The data for one of these events (16 October 2015, 13:07 UT) are presented here as an example of the electron-scale measurements of the reconnection diffusion/dissipation region around an X-line.

MMS measurements

The set of measurements made on each of the four MMS spacecraft are listed in Table 1. The improvement in time resolution for three-dimensional plasma distribution measurements was substantial: 30 ms for electrons and 150 ms for ions, as

[1]Southwest Research Institute, San Antonio, TX, USA. [2]University of New Hampshire, Durham, NH, USA. [3]University of California, Berkeley, CA, USA. [4]University of Maryland, College Park, MD, USA. [5]NASA, Goddard Space Flight Center, Greenbelt, MD, USA. [6]University of Colorado LASP, Boulder, CO, USA. [7]Blackett Laboratory, Imperial College London, London, UK. [8]West Virginia University, Morgantown, WV, USA. [9]Space Research Institute, Austrian Academy of Sciences, Graz, Austria. [10]Johns Hopkins University Applied Physics Laboratory, Laurel, MD, USA. [11]University of California, Los Angeles, CA, USA. [12]University of Delaware, Newark, DE, USA. [13]Swedish Institute of Space Physics, Uppsala, Sweden. [14]Royal Institute of Technology, Stockholm, Sweden. [15]Aerospace Corporation, El Segundo, CA, USA. [16]University of Colorado, Boulder, CO, USA. [17]Lockheed Martin Advanced Technology Center, Palo Alto, CA, USA. [18]Institut de Recherche en Astrophysique et Planétologie, Toulouse, France. [19]Department of Physics and Astronomy, Rice University, Houston, TX, USA. [20]Institute for Space and Astronautical Sciences, Sagamihara, Japan. [21]NASA, Marshall Space Flight Center, Huntsville, AL, USA.
*Corresponding author. Email: jburch@swri.edu

compared to previous resolutions in the few-second range. This improvement required the use of multiple analyzers rather than one spinning analyzer, resulting in stringent requirements on their absolute calibration and intercalibration.

Two benefits of this approach are the ability to make accurate measurements of currents and of electron drift velocities. Another advance is the accurate measurement of three-axis electric fields, which are crucially important for the investigation of reconnection. Data taken at the highest measurement resolution are referred to as burst-mode data, and all instruments operate in burst mode whenever the spacecraft are beyond a geocentric distance of 9 R_E on the dayside of Earth.

Table 1. Measurements made on each MMS spacecraft.

Fields	Three-dimensional electric and magnetic field measurements at time resolution of <1 ms (direct current) and waves to 6 kHz (*B*) and 100 kHz (*E*).
Fast plasma	Full-sky viewing of plasma electrons and ions at 32 energies (10 eV to 30 keV): electrons in 30 ms, ions in 150 ms.
Energetic particles	Full-sky viewing of ion and electron energetic particles (20 to 500 keV) with composition.
Plasma composition	Composition-resolved 3D ion distributions (1 eV to 40 keV) for H^+, He^{2+}, He^+, and O^+. Full sky at 10 s.
Potential control	Maintenance of spacecraft potential to ≤4 V using ion emitter.

A reconnection dissipation region encountered by MMS

Figure 1 shows summary plasma and field data for MMS1 at a time resolution of ~4 s on 16 October 2015. Because of data downlink limitations, only 2 to 4% of the burst-mode data can be transmitted to Earth. Data selection is made with two mechanisms: (i) an onboard system, which evaluates 10-s intervals of burst-mode data and prioritizes them according to expected reconnection signatures; and (ii) a scientist-in-the-loop system by which scientists view summary data (such as shown in Fig. 1) to select boundary crossings, flow jets, and other features that might have been

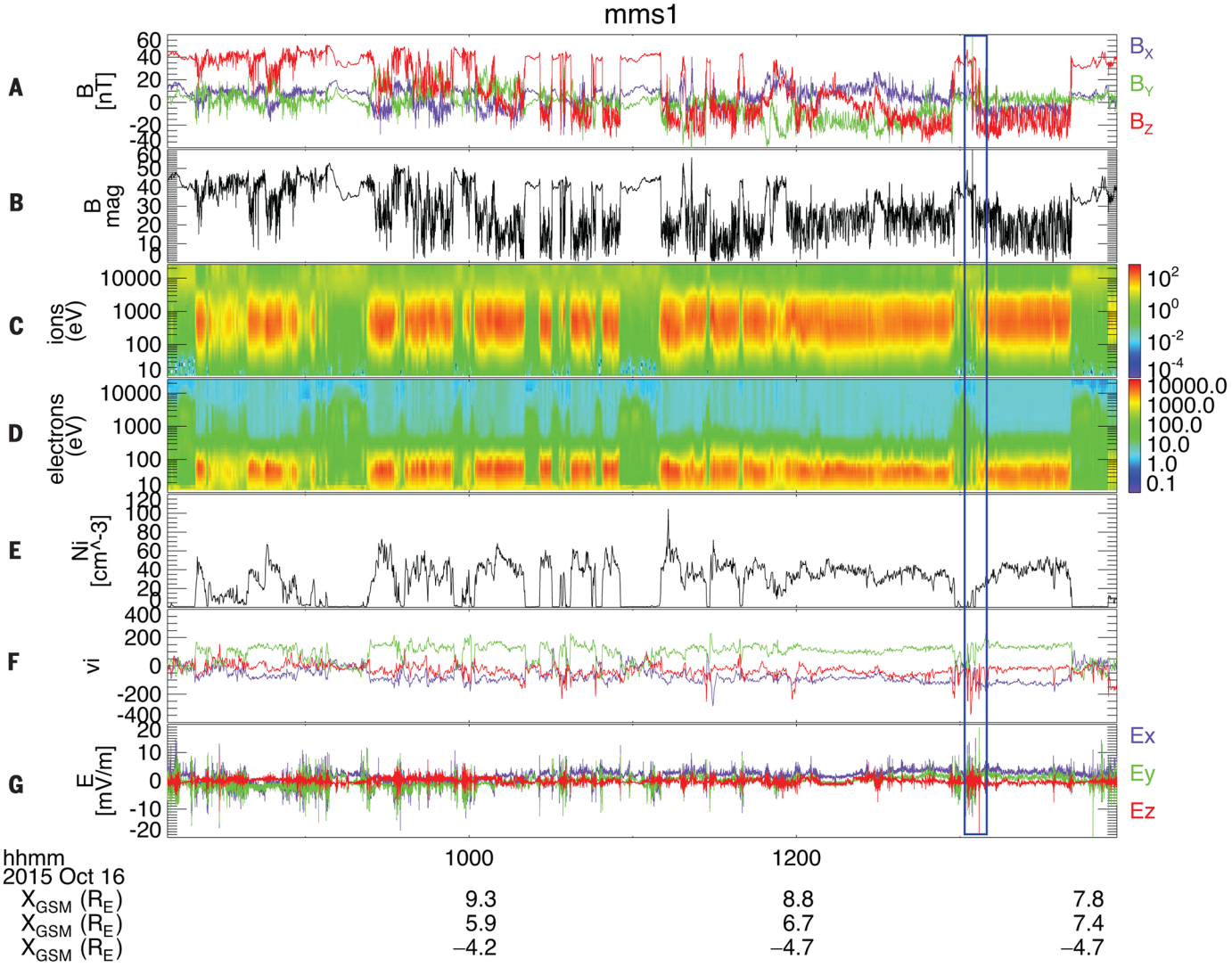

Fig. 1. Summary data in GSM (geocentric solar magnetospheric) coordinates from MMS1 on 16 October 2015. The GSM coordinate system has **X** toward the Sun, **Z** the projection of Earth's magnetic dipole axis (positive = north) onto the plane perpendicular to **X**, and **Y** completing the right-hand system (approximately toward dusk). (**A**) Magnetic field vector. (**B**) Magnetic field magnitude. (**C**) Ion energy-time spectrogram in energy flux (eV cm^{-2} sr^{-1} s^{-1}). (**D**) Electron energy-time spectrogram in energy flux (eV cm^{-2} sr^{-1} s^{-1}). (**E**) Ion density. (**F**) Ion velocity vector. (**G**) Electric field vector.

missed by the onboard system. Both mechanisms have been effective in identifying possible reconnection sites. Several magnetopause crossings were observed on this day. The particular event chosen for further analysis (near 13:07 UT) is noted by the blue box in Fig. 1.

Figure 2A shows the orbit as projected onto the ecliptic plane; Fig. 2B shows the tetrahedron occupied by the four spacecraft at 13:07:00 UT on 16 October 2015. During this time period, the separation among the spacecraft was controlled at 10 km. As shown in Fig. 2, MMS4 was located ~10 km south (toward –*Z*) of MMS2 and MMS3. The detailed electron distribution functions from the four spacecraft show evidence that the reconnection X-line was located to the north of MMS4 and to the south of MMS2 and MMS3. MMS1 was displaced toward negative values of *X* (toward Earth) so that as the magnetopause moved inward across the four spacecraft, MMS1 detected the dissipation region slightly later than the other three spacecraft (Fig. 2).

The 10-km average separation of the four spacecraft amounted to ~6 electron skin depths (the depth in a plasma to which electromagnetic radiation can penetrate) based on a magnetosheath (shocked solar wind) density of ~12 cm^{-3}. At such small spacecraft separations, the plasma and fields measured by the four spacecraft are nearly identical throughout most of the regions, except in thin electron-scale layers near the reconnection X-line.

Overview of two magnetopause crossings

Figure 3 shows MMS2 data during two encounters with the magnetopause over a period of almost 2 min. The magnetopause crossings are denoted by the two pairs of vertical blue dashed

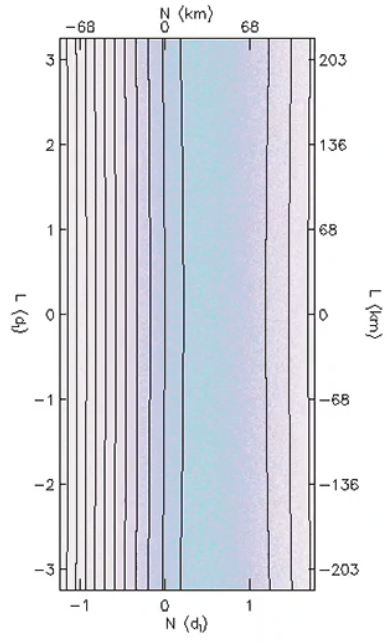

Movie 1. An electromagnetic particle-in-cell simulation with parameters corresponding to the event is performed with the *P3D* code (*27*). Particles are advanced using a relativistic Boris stepper with electromagnetic fields extrapolated to the particles' positions (*28*). Electromagnetic fields are evolved using the trapezoidal leapfrog scheme on Maxwell's equations with second-order spatial derivatives. The simulation is two-dimensional with periodic boundary conditions in both directions. Magnetic fields in the simulation are normalized to the magnitude of the *L* component of the magnetosheath magnetic field, 23 nT. Densities are normalized to the magnetosheath density, 11.3 cm^{-3}. Distances are normalized to 67.8 km (the magnetosheath ion inertial scale $d_{i,sh} = c/\omega_{pi,sh}$), and current densities to 0.270 $\mu A/m^2$. The initial conditions for the upstream values of the *L* and *M* components of the magnetic field, the densities, and the electron and ion temperatures on both sides of the current sheet are taken to match the event to the extent possible: $B_{L,ms}$ = 39 nT, $B_{L,sh}$ = 23 nT, $B_{M,ms} = B_{M,sh}$ = 2.278 nT, n_{ms} = 0.7 cm^{-3}, and n_{sh} = 11.3 cm^{-3}, where "ms" denotes the magnetospheric side and "sh" denotes the magnetosheath side. For the temperatures, magnetosheath values are $T_{p,sh}$ = 320 eV and $T_{e,sh}$ = 28 eV to match the MMS data. For the magnetosphere, the low density makes measuring temperatures difficult, so for the purposes of the simulation we defined the magnetospheric temperature as that required to balance total pressure in the fluid sense with a proton temperature 6 times the electron temperature: $T_{p,ms}$ = 1800 eV, $T_{e,ms}$ = 300 eV. No bulk flow of the upstream plasma is included in the initial conditions. The profiles for the initial conditions had double tanh profiles for the magnetic field and temperature, and the density profile is chosen to enforce pressure balance in the fluid sense. The domain size is 40.96 × 20.48 in normalized units and the grid scale is 0.01 in both directions. The time step is 0.001 in units of the magnetosheath inverse ion cyclotron frequency $\Omega_{ci,sh}^{-1}$ and is run until t = 40. The time step on the electromagnetic fields is half that of the particles to resolve light waves. The simulation is initialized with 500 particles per grid. The ion-to-electron mass ratio is 100 and the ratio of the speed of light to the initial magnetosheath Alfvén speed is 15 ($\omega_{pi,sh}/\Omega_{ci,sh}$ = 15); these differ from the realistic values of 1836 and 2000, respectively, but it is common to use smaller values for numerical expediency and is not expected to adversely affect the simulations. http://bcove.me/o51zgjqt.

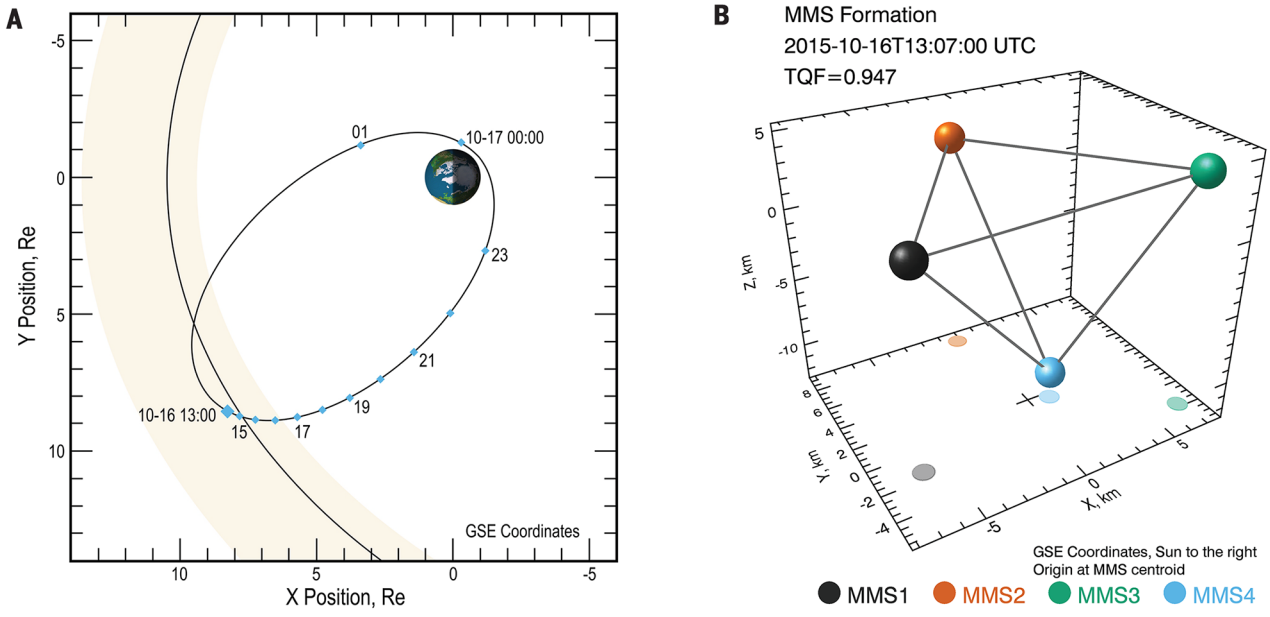

Fig. 2. Locations of the four MMS spacecraft during the magnetopause crossing investigated in this study. (**A**) Ecliptic-plane projection of MMS orbit in geocentric-solar-ecliptic (GSE) coordinates on 16 October 2015. The beige area is the MMS region of interest where burst-mode data are taken. Hours of the day are noted along the orbit. (**B**) MMS tetrahedral formation in GSE coordinates (**X** toward Sun, **Z** perpendicular to ecliptic plane, **Y** toward dusk).

lines. The diagram on the right side of Fig. 3 shows the typical structure of a magnetopause in which asymmetric reconnection is occurring, taken from a numerical plasma simulation shown in Movie 1 for the observed magnetosheath and magnetospheric conditions of the complete MMS magnetopause crossing at 13:05:30 UT. The diagram shows the northward magnetic field on the magnetosphere side of the boundary and the southward magnetic field on the magnetosheath side. The shear angle between the magnetosphere and magnetosheath magnetic fields is very large (~170°), implying a crossing with low guide field (the magnetic field component normal to the plane of the diagram). The converging plasma flows carry the two nearly oppositely directed magnetic field domains toward each other. An X-line directed normal to the plane of the diagram denotes the small region in the reconnection plane where the field lines interconnect, and this X-line is likely to extend by hundreds to thousands of kilometers in the east-west direction (*16*), which is why a large number of exhaust regions are typically crossed by spacecraft near the magnetopause. Another reason why reconnection events are routinely observed is the presence of the exhaust jets (red arrows) flowing northward and southward from the X-line and the nearby dissipation region (or diffusion region). Although the results of reconnection are readily observed with measurements at the fluid and ion scales, it is the electron-scale phenomena acting within the dissipation region that determine how reconnection occurs.

The color scale in the plasma simulation result in Fig. 3 shows the plasma current normal to the plane of the picture (J_M), which is nearly all due to fast-moving electrons generated by the reconnection process. The strong $-J_M$ values (shown in green) are highly localized at the dissipation region and X-line. The approximate path of the MMS tetrahedron, based on the plasma and field measurements, is shown by a blue dashed curve. Because the velocity of the magnetopause is approximately 100 times the spacecraft velocities, the MMS path shown is produced entirely by the motion of the magnetopause along L and N (directions defined in the Fig. 3 caption). For the magnetopause crossing centered at 13:07 UT, the spacecraft traversed both exhaust jet regions and passed through the dissipation region between them.

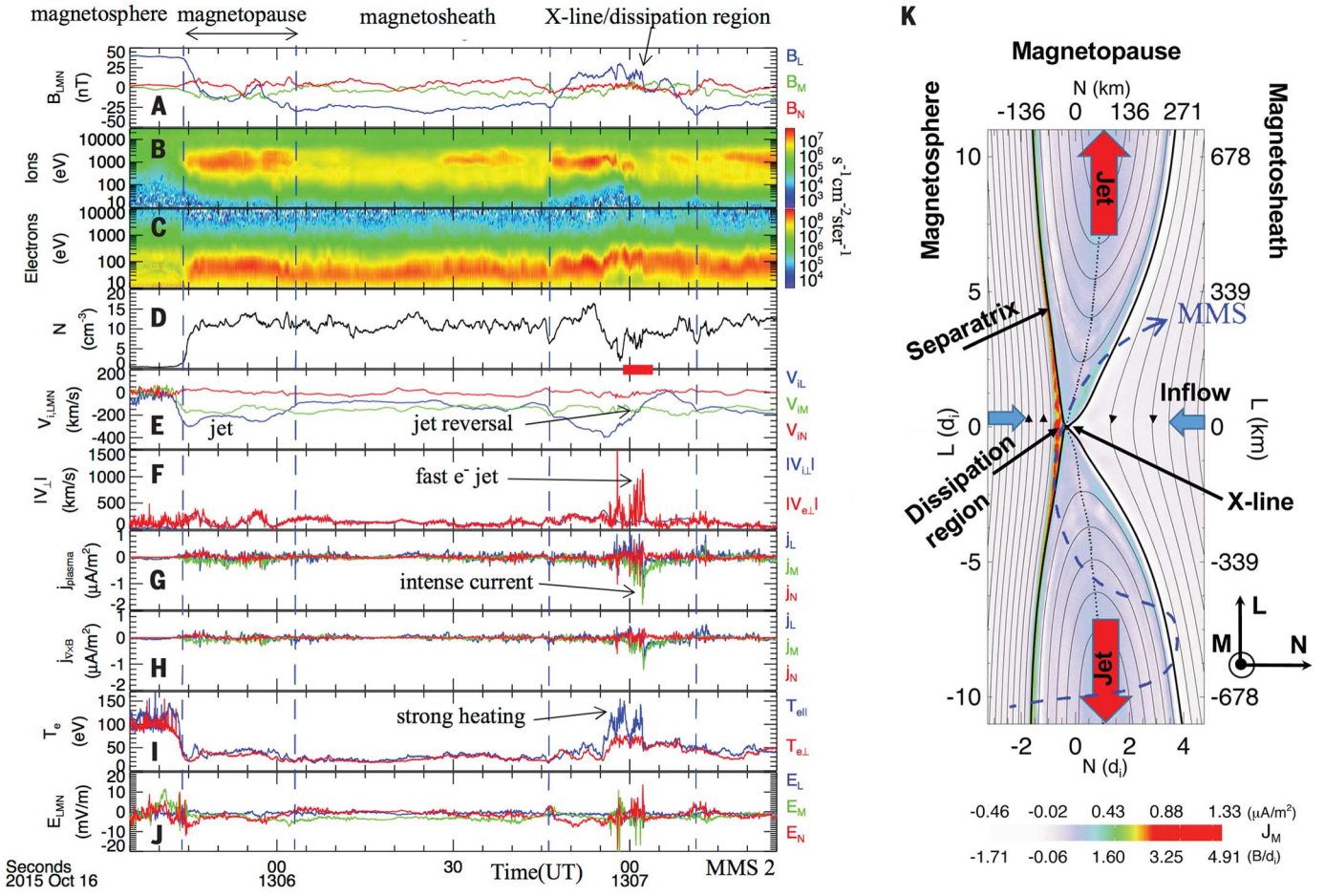

Fig. 3. Summary data for two magnetopause crossings of MMS2 on 16 October 2015. The crossings are shown by the vertical blue dashed lines. Boundary-normal coordinates (L, M, N) are used with N normal to the boundary and away from Earth, L perpendicular to N and in the plane of reconnection (nearly along the magnetospheric magnetic field direction), and M normal to the L, N plane (generally westward). These directions were determined from a minimum variance analysis of the magnetic field data between 13:05:40 and 13:06:09 UT. The (x, y, z) GSE components of the L, M, and N axes are L = (0.3665, −0.1201, 0.9226) GSE, M = (0.5694, −0.7553, −0.3245) GSE, and N = (0.7358, 0.6443, −0.2084) GSE. Panel data include (**A**) magnetic field vectors, (**B**) energy-time spectrogram of ion energy flux, (**C**) energy-time spectrogram of electron energy flux, (**D**) total plasma density, (**E**) ion flow velocity vectors, (**F**) magnitudes of electron and ion convection velocities, (**G**) current computed from velocity moments of ions and electrons, (**H**) current computed from ∇ × **B**, (**I**) parallel and perpendicular (to **B**) electron temperatures, and (**J**) electric field vectors. In the very-low-density region to the left of the first vertical blue dashed line, spacecraft charging effects on plasma moment calculations may affect the data. The diagram to the right is the result of a numerical plasma simulation (Movie 1) using parameters from the magnetopause crossing centered on 13:05:52 UT. Spatial coordinates in the diagram are shown both in kilometers and in ion diffusion lengths, $L(d_i)$. Color scale indicates J_M current density.

In comparison, the magnetopause crossing centered at about 13:05:52 UT occurred completely southward of the X-line in the exhaust, so that although it did include a traversal from well within the magnetosphere to well out into the magnetosheath, it did not encounter the dissipation region. This difference is best seen in the ion flow velocities in Fig. 3E, which when high in magnitude denote the exhaust jets. For the first magnetopause crossing, only southward jets ($V_{iL} < 0$) were observed, whereas for the second event (13:07 UT) both southward and northward jets were observed, with no gap between them. During the flow reversal near 13:07 UT, the reconnecting magnetic field (B_L) component was close to zero, suggesting that the spacecraft was in close proximity to the X-line. The red highlight bar at the top of Fig. 3E shows this reversal.

Another strong indicator of the dissipation region is the aforementioned $-J_M$ current, which can be seen in Fig. 3, G and H. The green trace is $-J_M$ (eastward current), which is predicted by the simulation to peak at the dissipation region. With MMS there are two ways to measure the currents: (i) $\nabla \times \mathbf{B}$ calculated from the magnetic field data from the four spacecraft (as in Fig. 3A), or (ii) $qn(\mathbf{V}_i - \mathbf{V}_e)$ using the computed moments of the ion and electron distribution functions, where q is the electronic charge and n is the plasma density. The correspondence between the two methods shown in Fig. 3 required a high level of calibration and cross-calibration of the various plasma instruments. Differences between the two methods at the smallest scales are mostly because even with 10-km separation, the currents are not completely uniform across the MMS tetrahedron, which is assumed in the $\nabla \times \mathbf{B}$ calculation.

The third strong indicator for a dissipation region is the enhancement of $-E_M$ (the reconnection electric field), which is shown by the green trace in Fig. 3J. The size of the E_M bursts of more than 10 mV/m is substantially larger than the correction due to X-line motion, which is on the order of 1 mV/m or less. There are also strong E_N components bracketing 13:07 UT, which are electric fields pointing outward and normal to the magnetopause. This normal component is predicted by simulations (*17*), and in a simple sense is caused by the deeper penetration into the magnetosphere of the magnetosheath ions because of their larger gyroradius relative to electrons with similar energies. The resulting charge separation produces an ambipolar electric field, E_N.

There are important differences between the reconnection exhaust at 13:05:52 UT and the region surrounding the X-line near 13:07 UT. First, as shown in Fig. 3I, the degree of electron heating (relative to the magnetosheath temperature) near the X-line ($\Delta T_{e||} \sim 120$ eV) is substantially higher than the heating in the exhaust ($\Delta T_{e||} \sim 20$ eV). Second, the electron flow speed perpendicular to the magnetic field, which largely tracks the ion perpendicular speed in the magnetosheath and the exhaust, significantly exceeds the ion flow speed near the X-line (Fig. 3F), resulting in a current that is much larger near the X-line than in the exhaust. These differences further support the identification of the X-line regions near 13:07 UT.

Details of plasma and field observations from MMS2

Figure 4 shows the 4 s marked with the red bar in Fig. 3E of MMS2 data near the X-line. Figure 4A shows that a deep magnetic field minimum occurred just after 13:07:02.4 UT; Fig. 4B shows a strong plasma current (J_M) starting at 13:07:02.1 UT (on the magnetosphere side of the X-line) and extending through the minimum magnetic field. Figure 4C shows vector electric fields. Inside the $-J_M$ current layer, the E_N component, which points outward from the magnetopause as described above, is the strongest. It is also noteworthy that E_M, the reconnection electric field, is negative, as is the J_M current. Figure 4D shows a comparison between $\mathbf{E}_M$ and $-(\mathbf{V}_e \times \mathbf{B})_M$. There is excellent agreement except near the dissipation region. Figure 4E shows the electric field component parallel to $\mathbf{B}$, which is strongest in the region of the J_M plasma current. Figure 4F shows $\mathbf{J} \cdot \mathbf{E}'$, where $\mathbf{E}' = \mathbf{E} + \mathbf{V}_e \times \mathbf{B}$, along with its parallel and perpendicular components. $\mathbf{J} \cdot \mathbf{E}'$ has been referred to as the "dissipation quantity" in simulation results (*18*). The plot in Fig. 4F shows clearly that the reconnection dissipation is caused by the strong $-J_M$ current and $-E_M$ electric field, which are perpendicular to $\mathbf{B}$ in the dissipation region as $\mathbf{B}$ is dominated by B_L in that region. Because reconnection is known to be a dissipative process that converts magnetic energy to heat and particle kinetic energy, the observation that $\mathbf{J} \cdot \mathbf{E} \approx J_M E_M > 0$ provides a form of "smoking gun" for a reconnection dissipation region.

Shown in Fig. 4, G to I, are energy-time spectrograms of electrons moving parallel, perpendicular, and antiparallel to the local magnetic field direction, respectively. In the region of dissipation (13:07:02.15 to 13:07:02.29 UT), the parallel fluxes shift to lower energies, the perpendicular fluxes rise in intensity and shift to lower energies, and the antiparallel fluxes remain at high energies. All of the fluxes drop to lower magnetosheath levels after exiting the dissipation region. The electron velocity-space distribution functions in Fig. 4, J to L, show three cuts through 3D distributions at 30-ms intervals through the dissipation region. Figure 4J shows cuts perpendicular to $\mathbf{B}$, where $V_{perp1} = (\mathbf{b} \times \mathbf{v}) \times \mathbf{b}$ and $V_{perp2} = -\mathbf{v} \times \mathbf{b}$ ($\mathbf{b}$ and $\mathbf{v}$ are unit vectors of the magnetic field and the electron velocity moment, respectively). Shown in Fig. 4, K and L, are two orthogonal cuts containing the magnetic field direction V_{para}.

Before MMS, the best 3D plasma measurement resolution was 3 s; that is, only a single plasma distribution would have been measured in such a brief interval. In comparison, MMS measured 26 ion distributions and 133 electron distributions in this interval. Movie 2 shows all of the MMS2 electron velocity-space distributions in video form for a 3-s interval centered in Fig. 4. The movie demonstrates that the 30-ms time resolution of MMS is necessary for performing this type of definitive investigation of the reconnection dissipation region.

The first column of distribution functions (on the magnetosphere side of the X-line) shows a crescent-shaped distribution in the perpendicular plane centered along the $+V_{perp1}$ axis in Fig. 4J, parallel heating in Fig. 4, K and L, along with a vertical cut through the crescent along $+V_{perp1}$ in Fig. 4K. This type of crescent-shaped distribution has been predicted from a simulation (*9*) that showed reduced distribution functions (integrated along V_{para}). In that simulation, the electrons in the crescent population were described as "meandering particles" consisting of accelerated magnetosheath electrons. Subsequent distribution functions in Fig. 4J show that as the X-line is approached along the path sketched in Fig. 3, the crescent-shaped distribution wraps around the origin and becomes a ring, which moves to lower energies. This energy shift is shown in the spectrogram in Fig. 4H.

Shown in Fig. 4, K and L, is a result that had not been predicted: the formation of a crescent-shaped distribution along V_{para}, indicating the transition of the perpendicular crescent electrons to field-aligned flow. Such a transition is strong evidence for the opening of magnetic field lines. At the end of the dissipation-region interval, the parallel crescent also begins to wrap around the origin and move to lower energies, as shown by the spectrogram in Fig. 4G. The crescent electrons are moving along $\mathbf{B}$ ($+V_{para}$) while the electrons along $-V_{para}$ continue to show the electron-heating feature (the elongation along $-V_{para}$), which extends to higher energies than the crescent population. The direction of the field-aligned flow of the crescent electrons indicates that MMS2 has moved above the X-line while still within the dissipation region (Fig. 3K). Because the electron spectrograms in Fig. 4, G to I, plot energy flux, they are much more sensitive to the high-energy parts of the distribution, and this fact explains why the antiparallel energy fluxes in Fig. 4I remain level throughout the dissipation region.

In summary, the data in Fig. 4 establish that MMS2 passed through a reconnection dissipation region around an X-line. The flow directions shown in the electron velocity-space distributions (crescent shifting from perpendicular to along $\mathbf{B}$) suggest that MMS2 moved northward from approximately the same L location as the X-line. Parallel electric fields (Fig. 4E) also occur in the dissipation region. In addition, there is a strong normal electric field, E_N, which may be related to the normal electric field predicted theoretically to result from magnetopause pressure gradients along the entire magnetopause (*19*). The crescent-shaped distributions are due to finite Larmor radius effects of magnetosheath electrons that have been accelerated toward the magnetosphere by E_N (Fig. 4C) in the weak magnetic field region near the X-line. This Larmor motion, together with acceleration by the reconnection electric field, results in a net out-of-plane electron bulk motion or electron current $-J_M$ that is observed (Fig. 4B). As the high-density magnetosheath electrons penetrate more deeply into the region

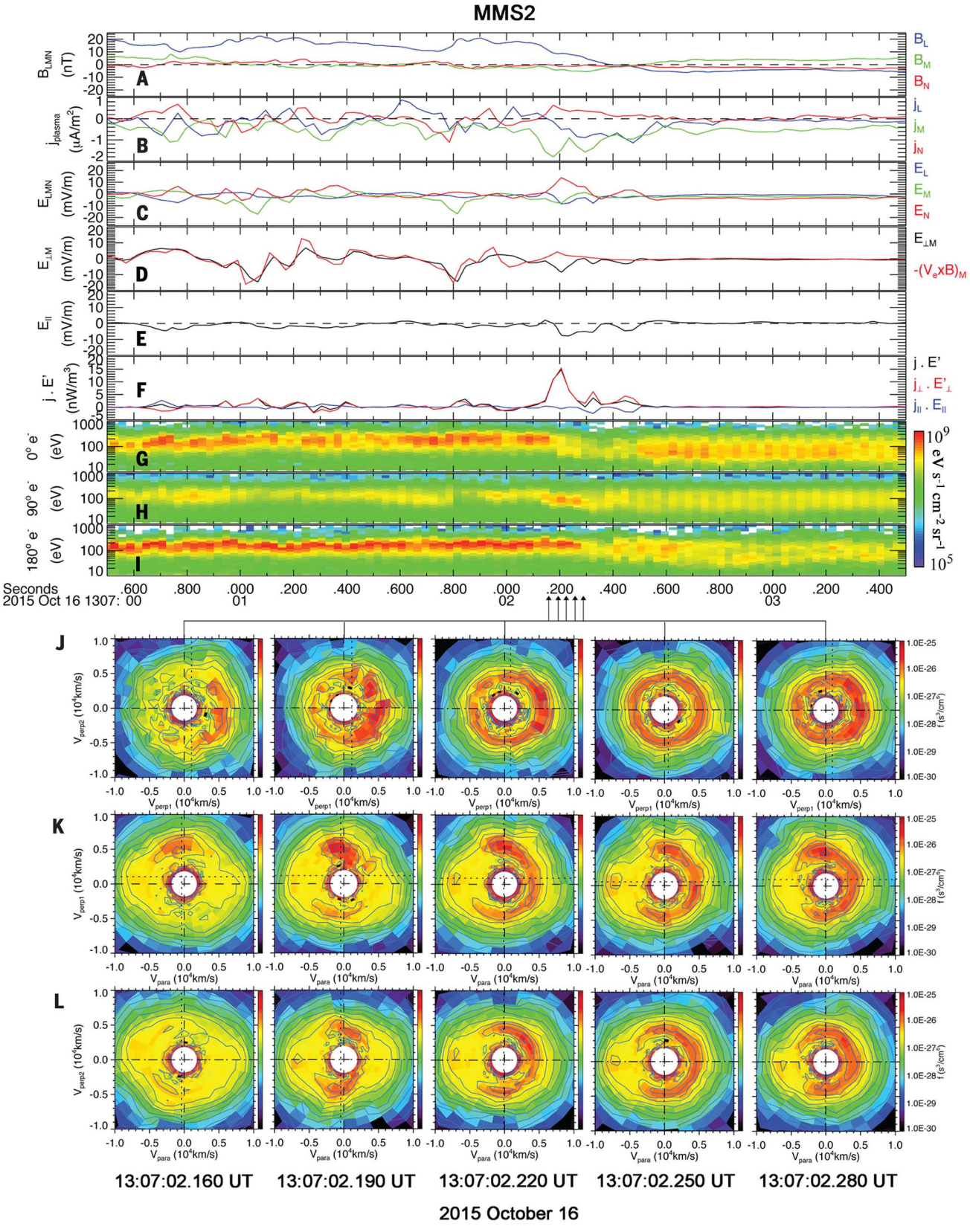

Fig. 4. MMS2 plasma and field data on 16 October 2015. (**A**) Magnetic field vector. (**B**) Currents from plasma measurements. (**C**) Electric field vector. (**D**) Comparison of *M* component of **E** and $-\mathbf{V}_e \times \mathbf{B}$. (**E**) $E_{||}$. (**F**) $\mathbf{J} \cdot \mathbf{E}$. (**G**) Electron energy-time spectrogram (pitch angle = 0° to 12°). (**H**) Electron energy-time spectrogram (pitch angle = 84° to 96°). (**I**) Electron energy-time spectrogram (pitch angle = 168° to 180°). (**J**) Electron velocity-space distribution (V_{perp1}, V_{perp2}). (**K**) Electron velocity-space distribution (V_{para}, V_{perp1}). (**L**) Electron velocity-space distribution (V_{para}, V_{perp2}). V_{perp1} is in the $(\mathbf{b} \times \mathbf{v}) \times \mathbf{b}$ direction, which is a proxy for $\mathbf{E} \times \mathbf{B}$.

with $B_L > 0$, they gain more energy from E_N, and this effect can be clearly seen by comparing the first and fifth columns of Fig. 4J. Because the X-line moved along the N direction across the spacecraft tetrahedron, the energy of accelerated magnetosheath electrons increases from right to left in Fig. 4. As can be seen in Movie 2, the electron distributions at the magnetic field minimum (~13:07:02.45 UT) are isotropic at very low energy, indicating demagnetization, as would be expected. As the electrons move inward (Earthward) toward the dissipation region, they gain successively more energy as they cross the open field lines at the outer part of the dissipation region (parallel crescent) and then develop the highest-energy perpendicular crescent as the parallel crescent disappears at the inner part (the magnetosphere side) of the dissipation region.

Multi-spacecraft observations of the dissipation region

Figure 5 shows multi-spacecraft plasma and field data for the same 4-s time period as in Fig. 4. The vector magnetic field data in Fig. 5A show that MMS 2, 3, and 4 all passed through the magnetopause together, with MMS1 following them by ~0.2 s. The spatial scale (along the magnetopause normal direction) of the various electron layers can be estimated as follows: The consecutive detections by the four spacecraft of the B_L gradient at 13:07:02.2 to 13:07:02.4 reveal that this structure moved at a speed of ~45 km/s along the normal direction. Thus, the width of the region where seven crescent distributions (each sampled over 30 ms) were observed is ~9 km, or 6 electron skin depths. The region of strong dissipation is even narrower, as shown by the electric field measurements in Fig. 5.

All four spacecraft measured somewhat similar electric field and currents with important differences in their amplitudes and duration, particularly with the trailing MMS1. Shown in Fig. 5, B to D, are E_M, E_N, and $E_{||}$, respectively. Near the dissipation region, MMS2, MMS3, and MMS4 measured the perpendicular and parallel electric fields at various levels and strong J_M current. The strongest $\mathbf{J} \cdot \mathbf{E}'$ peak was detected by MMS2, indicating its deepest penetration into the dissipation region.

The same types of electron velocity-space distributions presented in Fig. 4 for MMS2 were observed by MMS3 and MMS4. In Fig. 5, H to J, MMS4 distributions are shown in the first column, and MMS3 distributions are displayed in the other three columns. The first column of Fig. 5H shows that as MMS4 was entering the dissipation region, it saw the perpendicular crescent nearly wrapped around the origin as a ring. At the same time, Fig. 5J shows the formation of a parallel crescent as in Fig. 3, but in this case, it is centered on the $-V_{\text{para}}$ axis. This shift indicates that MMS4 was located below (or southward of) the X-line, which, as noted before, is consistent with its location shown in Fig. 2B. Also consistent with Fig. 2B are the parallel crescents that form in the third and fourth columns of Fig. 5, I and J, which are centered along the $+V_{\text{para}}$ axis, as was the case with MMS2. This direction indicates that MMS3, like MMS2, was located above (or northward of) the X-line. Exactly as for MMS2, the MMS3 perpendicular crescent in the second column of Fig. 5H appears first without a corresponding parallel crescent, but then evolves toward a ring in columns 3 and 4 as the parallel crescents develop.

Energetic electron evidence for the opening of magnetic field lines

For the analysis of magnetopause reconnection, very-high-energy electron features can be a valuable adjunct to analyses of lower-energy particles, because such electrons still have relatively small gyroradii (relative to the large-scale current sheet thickness) and are not expected to be perturbed by the strong electric fields in the vicinity of the electron diffusion region. The complex magnetic geometries of a reconnection site are expected to redirect energetic electrons in a fashion that reflects the magnetic geometry and topology of the small region. Interesting energetic electron signatures were indeed observed in the vicinity of the X-line by the Fly's Eye Energetic Particle Spectrometer (FEEPS), a part of the Energetic Particle Detector (EPD) investigation (*20*, *21*). The bottom panel of Fig. 6 shows the magnetic field data and identifies the location of the electron dissipation region (EDR). The top panel shows a pitch-angle distribution of >50-keV electrons, in which particles that travel parallel and antiparallel to the magnetic field are respectively located near the bottom and the top of the plot, and particles that gyrate nearly perpendicular to the magnetic field are near the vertical center of the plot. Our expectation has been that near an EDR, electrons might stream outward from the energetic particle populations residing on the Earthward side toward the magnetosheath side along field lines that are reconnected close to the EDR. Electrons are indeed streaming along field lines, and in the context of the spacecraft trajectory relative to the EDR developed elsewhere in this paper (Fig. 3K), the electrons appear to be traveling away from Earth. Specifically, starting around 13:06:55 UT, enhanced fluxes of >50-keV electrons were streaming primarily in the parallel direction with respect to the magnetic field and away from the Earthward side, based on the inferred location of the EDR. After MMS passed through the EDR around 13:07:02 UT, these electrons exhibited streaming in the magnetically opposite direction, predominantly antiparallel to the magnetic field, but the inferred trajectory of the spacecraft through the EDR (Fig. 3K) indicates that the electrons are again traveling away from Earth. These observations lend support to the idea that field lines connecting the magnetosphere and magnetosheath sides are generated through the reconnection process over small spatial scales dictated by electron processes.

Note that the time resolution of FEEPS (2.5 s) does not allow measurements within the EDR, but rather shows the reversal of the magnetic field–aligned motion of the >50-keV electrons from southward of the EDR to northward of it as MMS2 made this traversal. In this sense, the FEEPS data provide independent confirmation of the opening of magnetic field lines across the EDR, as deduced from the appearance of the parallel crescent in the low-energy electron data.

Data interpretation

The existence of the crescent-shaped electron distributions in the plane perpendicular to **B**, as shown in Figs. 4 and 5, can be explained conceptually as follows. There is typically a large ion pressure gradient across the magnetopause. During magnetic reconnection, this pressure gradient

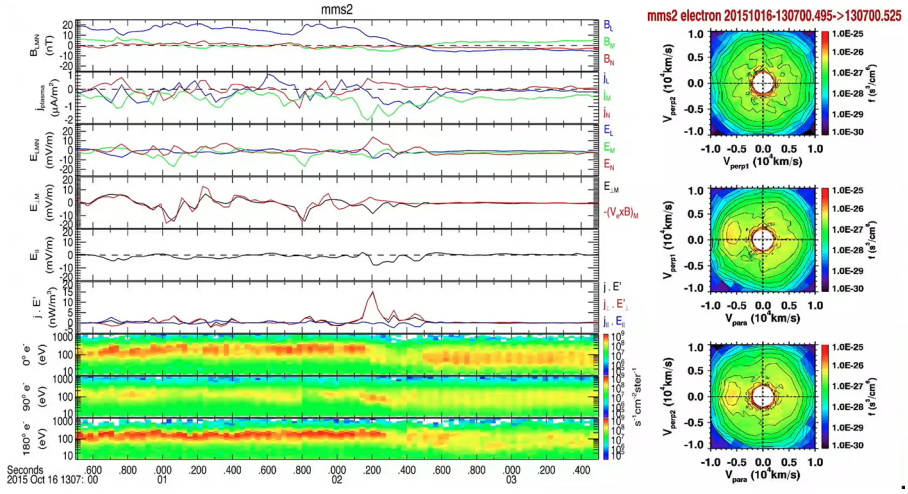

Movie 2. Three-second segment of burst-mode electron distributions keyed to a plot of plasma and field data covering the same time period as Fig. 4. One hundred electron velocity-space distributions are shown over this period. Previous missions that used the spacecraft spin to cover the full sky could only acquire one or fewer distributions over a time period of this length. This factor of 100 increase in electron time resolution is an important reason why MMS is able to investigate the electron-scale physics of reconnection. http://bcove.me/9fkcpfn1.

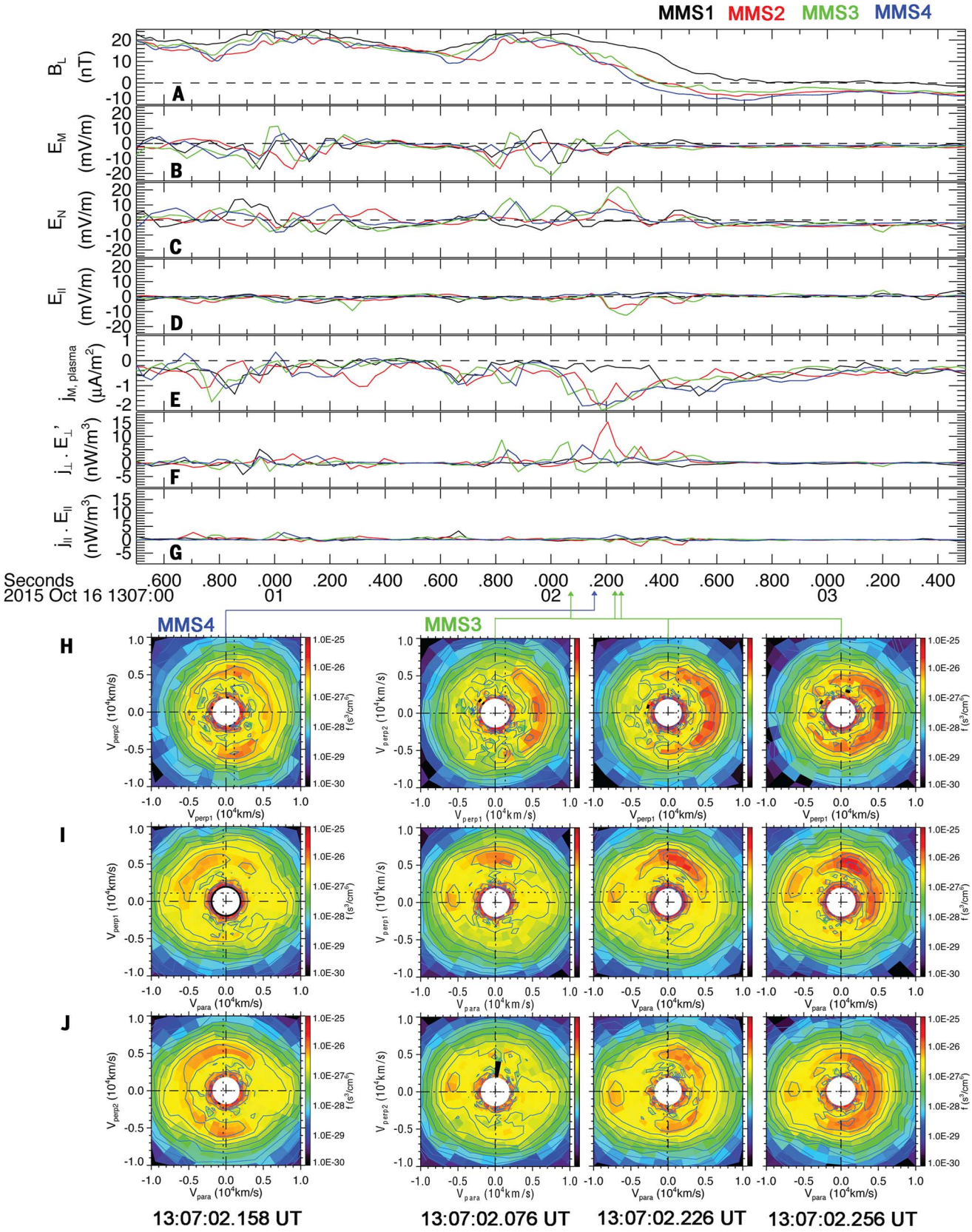

Fig. 5. Line plots of MMS field data from all four spacecraft on 16 October 2015. At the bottom are electron velocity-space distributions for MMS4 and MMS3. Panels are as in Fig. 4, except that the electron energy-time spectrograms are not shown. The parallel crescent in (J) for MMS4 is oriented in the opposite direction to that of MMS3, which is consistent with MMS4 being southward of the X-line and MMS3 being northward of it so that the electron flows are in opposite directions.

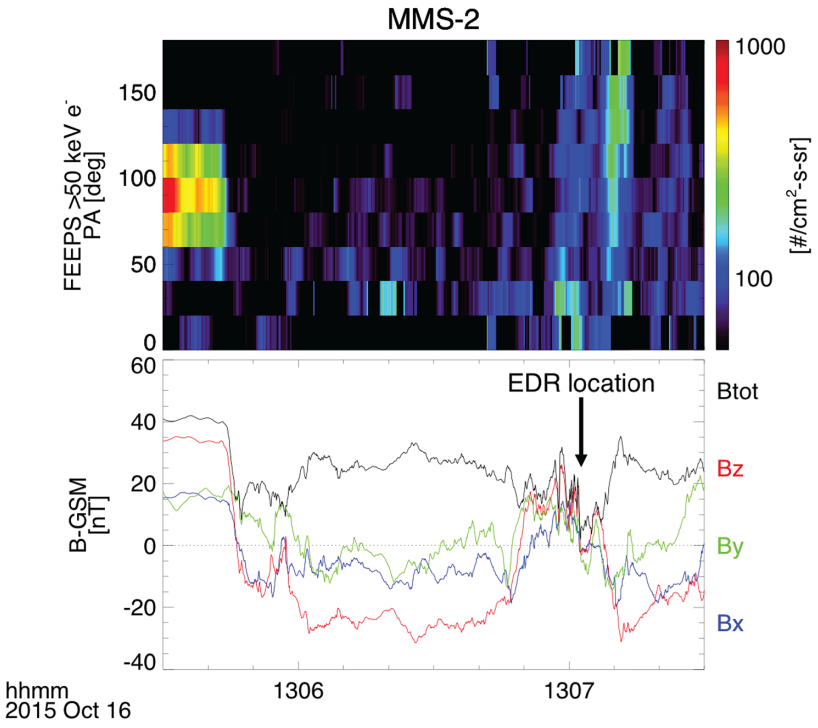

Fig. 6. Energetic electron data measured by FEEPS. Top: Pitch angle versus time spectrogram of energy flux carried by ~50-keV electrons. Bottom: Magnetic vectors in GSM coordinates and magnetic field magnitude.

produces a large normal electric E_N in an *LMN* coordinate system that points toward the Sun. This electric field balances the ion pressure gradient and keeps ions flowing from the magnetosheath from penetrating the magnetosphere. In the vicinity of the X-line, E_N modestly overlaps the null field region ($B_L = B_N = 0$). The strong out-of-plane current J_M during magnetopause reconnection actually peaks not at the X-line but displaced to the magnetosphere side of the X-line where E_N peaks. The high J_M is carried by high-velocity electrons with a crescent-shaped distribution in the V_M-V_N (perpendicular to B) plane that is symmetric across the V_M axis. This crescent distribution results from cusp-like orbits of electrons associated with the motion in the *M*-*N* plane controlled by $E_N(N)$ and $B_L(N)$ (*22*, *23*). The motion is similar to that of pickup ions in the solar wind (*24*). Electrons around $B_L = 0$ are accelerated toward the magnetosphere by E_N. As they gain energy, B_L causes them to turn in the M direction. Eventually they turn around, reaching a peak velocity along M that is around twice the $\mathbf{E} \times \mathbf{B}$ velocity $V_{EB} = cE_N/B_L$. The electrons return to $B_L = 0$ with zero velocity (ignoring their thermal spread) and repeat their cusp-like motion. The electron distribution function can be calculated analytically. With increasing distance from the null region to the turning point in N, it transitions from a hot thermal distribution to a horseshoe-like distribution (with more particles at higher V_M and a depletion of particles around V_M, $V_N = 0$) and then to a crescent centered at a velocity V_M that increases with distance into the region of high E_N and narrows in the V_M direction.

As the magnetopause moves inward in this event, the crescent-shaped electron population enters a region of very weak magnetic field containing open field lines in the inner part of the electron exhaust. In the exhaust region, newly reconnected field lines move rapidly away from the X-line northward and southward—a phenomenon that has been described as a double slingshot (*1*) or simply a magnetic slingshot (*2*). It is likely that these exhaust region dynamics are responsible for redirection of the perpendicular crescents into the observed parallel crescents. Although the perpendicular crescents (averaged over V_{parallel}) were predicted in simulations (*9*), the parallel crescents have not been. Their direct observation by MMS therefore represents a new target for simulations.

Summary and implications

The MMS mission, which was designed to perform a definitive experiment on magnetic reconnection in space, has investigated electron-scale physics in an encounter with the dissipation region near a reconnection X-line at Earth's magnetopause. The high temporal resolution and accuracy of the MMS plasma and field measurements were both necessary and sufficient for the investigation of the electron physics controlling reconnection.

Using measurements of plasma currents and reconnection electric fields, we have shown that $\mathbf{J} \cdot \mathbf{E}' > 0$ in the vicinity of the X-line, as predicted for the dissipative nature of reconnection. Electron distribution functions were found to contain characteristic crescent-shaped features in velocity space as evidence for the demagnetization and acceleration of electrons by an intense electric field near the reconnection X-line. MMS has directly determined the current density based on measured ion and electron velocities, which allowed the resolution of currents and associated dissipation on electron scales. These scales are smaller than the spacecraft separation distances and hence smaller than currents that can be determined by $\nabla \times \mathbf{B}$. The X-line region exhibits electron demagnetization and acceleration (by both E_N and E_M), which results in intense J_M current that is carried by the crescent-shaped electron distributions. Kinetic simulations had predicted some elements of the crescent distributions near the X-line, which raises the prospect of active interplay between theory and experiment, because the two techniques are now on a similar footing. The MMS measurements have led to discoveries about the evolution of electron acceleration in the dissipation region, as well as the escape of energized electrons away from the X-line into the downstream exhaust region. The latter was detected by at least two MMS spacecraft located on opposite sides of the X-line. The observed structures of the normal electric field and electron dynamics near the X-line by the four spacecraft are highly variable spatially and/or temporally, even on electron scales.

Among the implications of this initial MMS experiment is the discovery that the X-line region is important not only for the initiation of reconnection (breaking of the electron frozen-in condition), but also for electron acceleration and energization, leading to much stronger electron heating and acceleration than seen in the downstream exhaust. The details of the electron distribution functions, which show the rapid transition (within 30 ms) of the perpendicular crescent distributions to parallel crescents, provide experimental evidence for the opening up of magnetic field lines while also demonstrating that it is the electron dynamics that drives reconnection. Because of the importance of reconnection in many astrophysical and laboratory environments and the improvement achieved by its measurement resolution (*25*, *26*), MMS has opened up a new window on the universal plasma process of magnetic reconnection.

Materials and methods

The science phase of MMS began on 1 September 2015, when the orbit apogee precessed beyond the dusk meridian toward the dayside, after which it skimmed the magnetopause for 6 months. The scientific strategy was to position the four spacecraft in a tetrahedral formation at radial distances from 9 to 12 R_E, first at the ion scale (160 km) and progressing to the smaller electron scale (10 km), so that magnetic reconnection could be investigated as the magnetopause crossed back and forth across the tetrahedron in response to variations in the solar wind dynamic pressure. This strategy bore fruit as several magnetopause crossings were observed on most days, with many of these crossings showing evidence for magnetic reconnection based on the appearance of plasma jetting. A

small subset of these reconnection events was sampled directly when the MMS spacecraft crossed near or through the electron dissipation region within which magnetic energy is converted to particle kinetic energy. Effective sampling at the electron scale requires measurements at the highest instrument data rate, termed a "burst mode." Whenever the spacecraft are between 9 and 12 R_E (the region of interest), all instruments are run at their maximum data rates.

Because of data downlink volume limitations coupled with the unprecedentedly high internal data rate of the MMS instruments, careful selection of data to be downlinked is necessary. Two methods are used for the downlink data selection, both of which involve the use of a 96-GB onboard memory, which contains all the burst-mode data for two or more orbits of MMS. The first method of data selection involves the reporting of data evaluations by each instrument on a 10-s time scale, resulting in figures of merit for each interval, which are combined to generate a spacecraft figure of merit. These figures of merit are transmitted to the ground along with summary data for entire orbits. The summary data are similar to those shown in Fig. 1. Aggregate figures of merit for the four spacecraft are combined with ground software to generate a mission-level figure of merit. These automatically generated figures of merit then determine the priorities by which burst data are transmitted during the next ground contact.

The second data downlink selection method builds on the first one by using a scientist-in-the-loop to examine the figures of merit and the summary data for each day, with the goal of optimizing the data downlink selection by either adjusting the figures of merit or identifying new high-priority intervals that were not selected by the onboard system. Both systems are effective and both are being used throughout the mission. The data from all the independent sensors on each satellite, and between the four satellites, are intensively intercalibrated (*25*, *26*).

Beginning on 1 March 2016, the entire MMS data set has been available online at https://lasp.colorado.edu/mms/sdc/public/links/. Fully calibrated data are placed online at this site within 30 days of their transmission to the MMS Science Operations Center. The data are archived in the NASA Common Data Format (CDF) and so can be plotted using a number of different data display software packages that can use CDF files. A very comprehensive system called the Space Physics Environment Data Analysis System (SPEDAS) is available by downloading http://themis.ssl.berkeley.edu/socware/bleeding_edge/andselectingspdsw_latest.zip. Training sessions on the use of SPEDAS are held on a regular basis at space physics–related scientific meetings. All of the data plots in this paper were generated with SPEDAS software applied to the publicly available MMS database, so they could readily be duplicated.

REFERENCES AND NOTES

1. J. L. Burch, J. F. Drake, Reconnecting magnetic fields. *Am. Sci.* **97**, 392–399 (2009). doi: 10.1511/2009.80.392
2. G. Paschmann *et al*., Plasma acceleration at the Earth's magnetopause: Evidence for reconnection. *Nature* **282**, 243–246 (1979). doi: 10.1038/282243a0
3. M. Øieroset, T. D. Phan, M. Fujimoto, R. P. Lin, R. P. Lepping, In situ detection of collisionless reconnection in the Earth's magnetotail. *Nature* **412**, 414–417 (2001). doi: 10.1038/35086520; pmid: 11473310
4. F. S. Mozer, S. D. Bale, T. D. Phan, Evidence of diffusion regions at a subsolar magnetopause crossing. *Phys. Rev. Lett.* **89**, 015002 (2002). doi: 10.1103/PhysRevLett.89.015002; pmid: 12097047
5. G. Paschmann, S. J. Schwartz, C. P. Escoubet, S. Haaland, Eds., *Outer Magnetospheric Boundaries: Cluster Results* (Springer, 2005).
6. A. Vaivads *et al*., Structure of the magnetic reconnection diffusion region from four-spacecraft observations. *Phys. Rev. Lett.* **93**, 105001 (2004). doi: 10.1103/PhysRevLett.93.105001; pmid: 15447408
7. T. Nagai *et al*., Construction of magnetic reconnection in the near-Earth magnetotail with Geotail. *J. Geophys. Res.* **116**, 4222 (2011). doi: 10.1029/2010JA016283
8. J. L. Burch, T. E. Moore, R. B. Torbert, B. L. Giles, Magnetospheric Multiscale overview and science objectives. *Space Sci. Rev.* **199**, 5–21 (2016). doi: 10.1007/s11214-015-0164-9
9. M. Hesse, N. Aunai, D. Sibeck, J. Birn, On the electron diffusion region in planar, asymmetric, systems. *Geophys. Res. Lett.* **41**, 8673–8680 (2014). doi: 10.1002/2014GL061586
10. L.-J. Chen, M. Hesse, S. Wang, N. Bessho, W. Daughton, Electron energization and structure of the diffusion region during asymmetric reconnection. *Geophys. Res. Lett.* **43**, 2405–2412 (2016). doi: 10.1002/2016GL068243
11. J. R. Shuster *et al*., Spatiotemporal evolution of electron characteristics in the electron diffusion region of magnetic reconnection: Implications for acceleration and heating. *Geophys. Res. Lett.* **42**, 2586–2593 (2015). doi: 10.1002/2015GL063601
12. N. Bessho, L.-J. Chen, J. R. Shuster, S. Wang, Electron distribution functions in the electron diffusion region of magnetic reconnection: Physics behind the fine structures. *Geophys. Res. Lett.* **41**, 8688–8695 (2014). doi: 10.1002/2014GL062034
13. P. A. Cassak, M. A. Shay, Scaling of asymmetric magnetic reconnection: General theory and collisional simulations. *Phys. Plasmas* **14**, 102114 (2007). doi: 10.1063/1.2795630
14. M. Yamada, J. Yoo, S. Zenitani, Energy conversion and inventory of a prototypical magnetic reconnection layer. In *Magnetic Reconnection*, W. Gonzalez, E. Parker, Eds. (Springer, 2016), pp. 143–179.
15. M. Yamada, R. Kulsrud, H. Ji, Magnetic reconnection. *Rev. Mod. Phys.* **82**, 603–664 (2010). doi: 10.1103/RevModPhys.82.603
16. T. D. Phan *et al*., Extended magnetic reconnection at the Earth's magnetopause from detection of bi-directional jets. *Nature* **404**, 848–850 (2000). doi: 10.1038/35009050; pmid: 10786785
17. P. L. Pritchett, Collisionless magnetic reconnection in an asymmetric current sheet. *J. Geophys. Res.* **113**, A06210 (2008). doi: 10.1029/2007JA012930
18. S. Zenitani, M. Hesse, A. Klimas, M. Kuznetsova, New measure of the dissipation region in collisionless magnetic reconnection. *Phys. Rev. Lett.* **106**, 195003 (2011). doi: 10.1103/PhysRevLett.106.195003
19. D. M. Willis, Structure of the magnetopause. *Rev. Geophys.* **9**, 953–985 (1971). doi: 10.1029/RG009i004p00953
20. J. B. Blake *et al*., The Fly's Eye Energetic Particle Spectrometer (FEEPS) sensors for the Magnetospheric Multiscale (MMS) Mission. *Space Sci. Rev.* **199**, 309–329 (2016). doi: 10.1007/s11214-015-0163-x
21. B. H. Mauk *et al*., The Energetic Particle Detector (EPD) investigation and the Energetic Ion Spectrometer (EIS) for the Magnetospheric Multiscale (MMS) Mission. *Space Sci. Rev.* **199**, 471–514 (2016). doi: 10.1007/s11214-014-0055-5
22. M. A. Shay *et al*., Kinetic signatures of the region surrounding the X-line in asymmetric (magnetopause) reconnection. *Geophys. Res. Lett.* 10.1002/2016GL069034 (2016). doi: 10.1002/2016GL069034
23. N. Bessho, L.-J. Chen, M. Hesse, Electron distribution functions in the diffusion region of asymmetric magnetic reconnection. *Geophys. Res. Lett.* **43**, 1828–1836 (2016). doi: 10.1002/2016GL067886
24. A. J. Coates, A. D. Johnstone, B. Wilken, K. Jockers, K.-H. Glassmeier, Velocity space diffusion of pickup ions from the water group at comet Halley. *J. Geophys. Res.* **94**, 9983–9993 (1989). doi: 10.1029/JA094iA08p09983
25. C. Pollock *et al*., Fast Plasma Investigation for Magnetospheric Multiscale. *Space Sci. Rev.* **199**, 331–406 (2016). doi: 10.1007/s11214-016-0245-4
26. R. B. Torbert *et al*., The FIELDS Instrument Suite on MMS: Scientific objectives, measurements, and data products. *Space Sci. Rev.* **199**, 105–135 (2016). doi: 10.1007/s11214-014-0109-8
27. A. Zeiler *et al*., Three-dimensional particle simulations of collisionless magnetic reconnection. *J. Geophys. Res.* **107**, 1230 (2002). doi: 10.1029/2001JA000287
28. C. K. Birdsall, A. B. Langdon, *Plasma Physics via Computer Simulation* (Taylor & Francis, 2004).

ACKNOWLEDGMENTS

The dedicated efforts of the entire MMS team are greatly appreciated. We are especially grateful to the leadership of C. Tooley, B. Robertson, and R. Black. Special thanks are due to C. Pankratz and K. Larsen of the University of Colorado for their leadership of the MMS Science Operations Center. Supported by NASA contract NNG04EB99C at Southwest Research Institute, which funded work at most of the co-author institutions in the United States. The IRAP contribution to MMS was supported by CNES. The Austrian contributions to the MMS mission are supported by grants from the Austrian Research Promotion Agency FFG. The UK work was supported by the UK Science and Technology Facilities Council through grants ST/K001051/1 and ST/N000692/1. The work by NASA GSFC authors was supported by the NASA Solar Terrestrial Probes program. The work of the GSFC-resident University of Maryland co-authors was supported by NASA Goddard Planetary Heliophysics Institute contract NNG11PL02A. Work at U.C. Berkeley was supported by NASA MMS-IDS grant NNX08AO83G through the University of California. Work at the University of Colorado by M.G. and D.N. was supported by NASA MMS-IDS Grant NNX08AO84G through the University of Colorado. Work at the Swedish Institute for Space Physics and the Royal Institute of Technology was supported by the Swedish National Space Board. Work at West Virginia University was supported by NSF grants AGS-0953463 and AGS-1460037 and by NASA grants NNX16AG76G and NNS16AF75G.

20 January 2016; accepted 3 May 2016
Published online 12 May 2016
10.1126/science.aaf2939

Electron-scale measurements of magnetic reconnection in space

J. L. Burch, R. B. Torbert, T. D. Phan, L.-J. Chen, T. E. Moore, R. E. Ergun, J. P. Eastwood, D. J. Gershman, P. A. Cassak, M. R. Argall, S. Wang, M. Hesse, C. J. Pollock, B. L. Giles, R. Nakamura, B. H. Mauk, S. A. Fuselier, C. T. Russell, R. J. Strangeway, J. F. Drake, M. A. Shay, Yu. V. Khotyaintsev, P.-A. Lindqvist, G. Marklund, F. D. Wilder, D. T. Young, K. Torkar, J. Goldstein, J. C. Dorelli, L. A. Avanov, M. Oka, D. N. Baker, A. N. Jaynes, K. A. Goodrich, I. J. Cohen, D. L. Turner, J. F. Fennell, J. B. Blake, J. Clemmons, M. Goldman, D. Newman, S. M. Petrinec, K. J. Trattner, B. Lavraud, P. H. Reiff, W. Baumjohann, W. Magnes, M. Steller, W. Lewis, Y. Saito, V. Coffey and M. Chandler (May 12, 2016)
Science **352** (6290), . [doi: 10.1126/science.aaf2939] originally published online May 12, 2016

Editor's Summary

Probing magnetic reconnection in space

Magnetic reconnection occurs when the magnetic field permeating a conductive plasma rapidly rearranges itself, releasing energy and accelerating particles. Reconnection is important in a wide variety of physical systems, but the details of how it occurs are poorly understood. Burch *et al.* used NASA's Magnetospheric Multiscale mission to probe the plasma properties within a reconnection event in Earth's magnetosphere (see the Perspective by Coates). They find that the process is driven by the electron-scale dynamics. The results will aid our understanding of magnetized plasmas, including those in fusion reactors, the solar atmosphere, solar wind, and the magnetospheres of Earth and other planets.

Science, this issue p. 10.1126/science.aaf2939; see also p. 1176

Science (print ISSN 0036-8075; online ISSN 1095-9203) is published weekly, except the last week in December, by the American Association for the Advancement of Science, 1200 New York Avenue NW, Washington, DC 20005.